Two sets of amino acids of the domain I of Cav2.3 Ca(2+) channels contribute to their high sensitivity to extracellular protons.

Thierry Cens, Matthieu Rousset, Pierre Charnet

Two sets of amino acids of the domain I of Cav2.3 Ca^{2+} channels contribute to their high sensitivity to extracellular protons.

Thierry Cens, Matthieu Rousset & Pierre Charnet

CRBM CNRS UMR 5237, Montpellier, France; CRBM, UMSF, Montpellier, France.

Running title: Role of domain I in the pH sensitivity of VGCC

Corresponding author: Thierry Cens, CRBM, 1919 Route de Mende, 34293 Montpellier, France; Tel: (33)-467-61-33-52; Fax: (33)-467-52-15-59; email: thierry.cens@crbm.cnrs.fr

ABSTRACT

Extracellular acidification decreases Ca^{2+} current amplitude and produces a depolarizing shift in the activation potential (Va) of voltage-gated Ca^{2+} channels (VGCC). These effects are common to all VGCC, but differences exist between Ca^{2+} channel types and the underlying molecular mechanisms remain largely unknown. We report here that the changes in current amplitude induced by extracellular acidification or alkalinisation are more important for Cav2.3 R–type than for Cav2.1 P/Q-type Ca^{2+} channels. This difference results from a higher shift of Va combined with a modification of channel conductance. Although involved in the sensitivity of channel conductance to extracellular protons, neither the EEEE locus nor the Divalent Cation Selectivity locus could explain the specificity of the pH effects. We show that this specificity involves two separate sets of amino acids within domain I of the Cavα subunit. Residues of the voltage sensor domain and residues in the pore domain mediate the effects of extracellular protons on Va and on channel conductance, respectively. These new insights are important for elucidating the molecular mechanisms that control VGCC gating and conductance and for understanding the role of extracellular protons in other channels or membrane-tethered enzymes with similar pore and/or voltage sensor domains.

Keywords: Voltage-gated Ca^{2+} channels, extracellular pH, conductance, gating.

INTRODUCTION

Substantial changes in the extracellular pH (pHo)[1] arise in the central nervous system under physiological and patho-physiological situations (see, for example [33]). These changes have a strong effect on the properties of many receptors and ion channels of the plasma membrane (see, for examples [13, 14]). Although both Low (LVA) and High (HVA) voltage-activated Ca^{2+} channels are affected by pHo changes [2, 22, 25, 30, 37], little is known about the effects of pHo variations on the different HVA channels (namely the L-, P/Q, N and R-types), since most of the studies have focused only on L-type Ca^{2+} channels. HVA channels are complexes formed by the association of the pore-forming Cavα subunit with auxiliary subunits, of which the most important are Cavβ and Cavα2δ [7]. Six of the seven different HVA Cavα subunits (Cav1.2, 1.3 and 1.4 (L-types), Cav2.1 (P/Q-type), Cav2.2 (N-type) and Cav2.3 (R-type)) are expressed in the central nervous system [32]. They display specific cellular and subcellular localizations and they are essential for cell excitability and synaptic transmission [3, 32]. Although all these channels are highly selective for Ca^{2+}, they present specific biophysical properties that mainly rely on the Cavα subunit and to a lesser extent on the associated Cavβ subunit (for the P-type Ca^{2+} channels for example [5, 23]). Extracellular acidification decreases current amplitude and shifts the current-voltage curve of all Cavα subunits, but quantitative differences exist among them [12]. Two mechanisms have been proposed to explain these effects. Protonation of glutamates of the EEEE locus, which forms with the Divalent Cation Selectivity (DCS) locus the selectivity filter localized in the P-loops of the Cavα subunit [8, 34], has been suggested to be responsible for the inhibition of current amplitude in L-type Cav1.2 Ca^{2+} channels [9, 20]. On the other hand, the pHo-induced shift of the activation potential (Va) has been attributed to the screening of the surface charges by extracellular protons [26]. However, surface charges are thought to be largely independent from the channel itself [15] and the EEEE locus is perfectly conserved in all the HVA Cavα subunits [24], thus leaving the differential pHo sensitivity of the various Cavα subunits largely unexplained.

In this study, we took advantage of the large difference in sensitivity to pHo between Cav2.1 and Cav2.3 Ca^{2+} channel subunits to decipher the molecular mechanisms of the effects induced by pHo changes. We show that this differential sensitivity is mediated by the Cavα domain I and we identified two subsets of amino acids within the voltage sensor domain and

[1] Abbreviations used in this paper : VGCC, voltage gated Ca^{2+} channels; HVA, High voltage-activated; LVA, Low voltage-activated; DCS, divalent cations selectivity; Va, activation potential; VSD, voltage sensor domain; pHo, extracellular pH; G, maximal whole cell conductance.

in the pore domain that are responsible for the pHo effects on Va and on channel conductance, respectively. These results provide new and important clues for understanding how extracellular protons can specifically modify the biophysical properties of a given channel.

MATERIALS AND METHODS

Molecular Biology.

All the subunits used in this study were from rat brain: $Ca_v2.1$ (Genbank accession number M64373), $Ca_v2.3$ (L15453), Cavβ2a (M80545) and Cavα2δ (M86621). The full-length Cav2.1 subunit was obtained by sequential ligations of nine fragments that correspond to the four domains and the five intracellular parts as previously described [5]. The mutants Cav2.1(TEQE) and Cav2.3(AAAA) have been previously described [8]. The cDNAs corresponding to the Cav2.3 domains (EI, EII, EII and EIV, with reference to α1E in the old nomenclature) were PCR amplified, subcloned into modified versions of the pBluescript cloning vector (Stratagene) and fully sequenced. A restriction site (EcoRI) used for domain swapping was introduced in the cDNAs of domain I of Cav2.1 and Cav2.3 (the position is marked by an arrow in Figure 6). The mutations H217A and H130/134A were introduced in the Cav2.3 domain I using the GeneEditor Site-Directed Mutagenesis System (Promega) and confirmed by sequencing. The chimeras Cav2.1(EI to EIV), Cav2.1(pore-E), Cav2.1(VSD-E) and the mutants Cav2.3(H217A) and Cav2.3(H130/134A) were then produced by ligation of the appropriate fragments. All subunits were subcloned in the pMT2 expression vector for injection in *Xenopus* oocytes.

Electrophysiology.

Xenopus oocytes were isolated as described [6] and injected with 10-20 nl of a mixture of Cavα + Cavβ + Cavα2δ (mol/mol/mol). After 2-4 days, macroscopic whole-cell currents were recorded under two-electrode voltage-clamp using a GeneClamp 500 amplifier (Molecular Devices) connected to the bath by a virtual bath-clamp head-stage and 3M KCl agar-bridges. Voltage and current electrodes were filled with 3M KCl and had a typical resistance of 0.5-1 MΩ. Contaminating endogenous Ca^{2+}-activated Cl^- currents were suppressed by injecting a BAPTA solution (100 mM BAPTA, 10 mM HEPES, 10 mM CsOH, pH 7.2 with CsOH) into oocytes before recordings. Voltage command, sampling, data acquisition and analysis were done using a Digidata 1200 and the pClamp software (Molecular Devices). All experiments were performed at room temperature. The bathing solutions had the following composition: 10 mM BaCl, 2 mM CsCl, 20 mM TEACl, 5 mM HEPES, 5 mM Tris, 5 mM MES, 50 mM N-methyl-D-glucamine (pHo was adjusted with HCl). The osmolarity of the different solutions was between 160 and 180 mosm.

Ba^{2+} currents were evoked by 400 ms-long depolarization steps from -60 to +40 mV applied every 30s (Figure 1), or by 400 ms-long voltage ramps from -80 to +80mV applied

every 15s, in both cases from a holding potential of -100 mV. For each oocyte, the current-voltage curves obtained at different pHo were fitted using the following equation:

$$I = G(V-Erev)/(1+\exp((V-Va)/k))$$

where I is the current amplitude measured during the depolarization to V, G is the maximal whole-cell conductance, Erev is the apparent reversal potential, Va is the potential for half activation and *k* is a slope factor. The current-voltage parameters obtained for wild type Cav2.1 and wild type Cav2.3 at different pHo are listed in Table 1. For each oocyte, the difference between the Va obtained at different pHo and at pHo = 7 (ΔVa) was determined and the mean values are in Table 2. Similarly, for each oocyte the ratio between the G obtained at different pHo and the G at pHo = 7 (G_x/G_7) was determined and the mean values are in Table 3. The G_x/G_7 values were reported against pHo and fitted with a Hill's equation. For each oocyte, we calculated the variation of the current amplitude produced by a shift of Va (ΔIv = G * ΔVa) and measured the variation of the current amplitude as the difference between the peak current amplitude at different pHo and at pHo = 7 (ΔI). We then determined the percentage of the variation of the current amplitude that resulted from the shift of Va (ΔIv/ΔI * 100) and averaged the values.

For single-channel recordings, the oocyte vitelline membrane was removed using forceps after immersion in a hypertonic solution (200 mM NaCl, 10 mM HEPES) and the oocyte was then placed in the recording chamber filled with a depolarizing solution (100 mM KCl, 5 mM HEPES, 10 mM EGTA, pH 7.2 adjusted with KOH; the osmolarity was ~250 mosmol). Coated (Sylgard®), fire-polished patch pipettes had a resistance of 8-12 MΩ when filled with the pipette solution containing 100 mM $BaCl_2$, 5 mM HEPES, 5 mM Tris (pH was adjusted with NaOH; ~290 mosmol). Cell-attached patch-clamp currents were recorded with an Axopatch 200B amplifier (Molecular Devices), low-pass filtered at 2 kHz and digitized at 10 kHz using a Digidata 1200 interface and stored on a computer using the Clampex software. The liquid junction potential was 1-3 mV and was thus neglected. Currents were analysed with the Clampfit software (Molecular Devices). Linear leak and capacitive transients were subtracted by means of the manual baseline adjustment command of Clampfit. Well-resolved channel openings were detected by a threshold analysis set at 50% of the elementary current. Channel conductance and open-time constants were calculated from Gaussian and multi-exponential fits of amplitude and open-time histograms, respectively, obtained at different voltages.

Results were expressed as means ± SEM. The statistical significance of the difference between two results was determined using the non-paired Student's *t* test set at the 0.05 level.

RESULTS

To decipher the molecular mechanisms underlying the effects induced by pHo changes on HVA Ca^{2+} channels, we first obtained traces of current and current-voltage curves for wild type Cav2.1 (Fig. 1 A) and wild type Cav2.3 (Fig. 1 B) at different extracellular pH (pHo). Changes in pHo modified the current amplitude in both Cav2.1 and Cav2.3 subunits, but the increase of the current amplitude at alkaline pHo or the decrease at acidic pHo was significantly more important for Cav2.3 than for Cav2.1 (Fig. 1). Nevertheless, the kinetics of current inactivation (not shown, but see the current traces in Fig. 1) and the reversal potentials (Table 1) obtained with both Cavα subunits were similar at different pHo. We could therefore exclude that the different pHo sensitivity of Cav2.1 and Cav2.3 was due to a specific pH-dependent modification of current inactivation or the involvement of a proton-carried or proton-induced current. It is noteworthy that the effects of the pHo variations were comparable when Ca^{2+} was used instead of Ba^{2+} and that the ICa/IBa ratio, which is specific for Cav2.1 and Cav2.3 [8], was also similar at pHo = 6, 7 and 8 (not shown). This suggests that the selectivity profile of both channels was not affected by the pHo changes. The magnitude of the activation potential shift (ΔVa) induced by pHo variations was larger for Cav2.3 than for Cav2.1 at either alkaline or acidic pHo (Fig. 1 and Table 2). Moreover, the ratios between the maximal whole-cell conductance (G) measured at pHo 6 or 8 and the G measured at pHo = 7 (G_x/G_7), were significantly more affected by pHo changes for Cav2.3 than for Cav2.1 (Table 3). We therefore concluded that pHo affects not only Va but also G and that these effects are stronger in Cav2.3 than in Cav2.1. We estimated that at pHo = 6 the Va shift contributed similarly to the change in current amplitude in Cav2.3 and Cav2.1 (66 ± 2 %, n = 10 and 64 ± 4 %, n = 16, respectively). However, at pHo = 8, G was marginally affected in Cav2.1 (Table 3) and the changes in current amplitude resulted only from the shift of Va. For Cav2.3, the Va shift contributed to the same extent at pHo = 8 than at pHo = 6 to the change in current amplitude (65 ± 4 %). Differences in the pHo sensitivity of both Va and G are therefore responsible of the difference in the current amplitude recorded with Cav2.1 and Cav2.3.

Changes in G could be due to a difference in the number of functional channels at the plasma membrane and/or changes in their open probability and/or unitary conductance. It is very unlikely that the changes in G resulted from a modification of the number of channels at the plasma membrane, because the increase/decrease of current amplitude was usually reached in less than one minute (not shown). The differences in G_x/G_7 values rather suggested an effect of pHo on single channel properties. To evaluate this possibility, we carried out

single channel recordings in Xenopus oocytes that expressed the Cav2.3 subunit in the presence of an extracellular solution at pHo = 7 or 10 (Fig. 2 A). While the open time distributions were only marginally affected (Fig. 2 B), single conductance increased from 16 ± 0.7 pA to 23.9 ± 0.9 pA upon increasing the pHo from 7 to 10 (Figs. 2 A and C). Although we cannot exclude a change of the open probability, we concluded that the change in G was mostly caused by the change of the unitary conductance.

In order to decipher the molecular mechanisms underlying the differential pHo sensitivity of these channels, we then applied voltage ramps on Xenopus oocytes rather than square pulses because this allowed us to test the effects of a large panel of extracellular solutions on a single oocyte (Fig. 3). The current-voltage parameters obtained with voltage ramps nicely fitted those obtained with square pulses for both Cavα subunits (Table 1). The ΔVa (Table 2) and G_x/G_7 (Table 3) values, as well as the ratio of peak current amplitudes (not shown), determined with voltage ramps were also similar to those obtained with square pulses. In our recording conditions, the use of voltage ramps was therefore well suited to study the effects of pHo changes and we confirmed that the ΔVa and G_x/G_7 values obtained with Cav2.1 were significantly different from those obtained with Cav2.3 at all tested pHo (Tables 2 and 3).

The EEEE locus is the main structure that governs channel conductance. This is also the only determinant so far implicated in the mediation of the effects of extracellular protons. However, this locus is not a good candidate to explain the differential sensitivity of the Cav2.1 and Cav2.3 channels to pHo, because it is perfectly conserved in both subunits. Since we have recently shown that the neighbouring DCS locus contributed to the specific conductance displayed by the different Cavα subunits [8], we wondered whether this site could also be involved in the specific effect of pHo. Mutation of the amino acids of the Cav2.3 DSC to alanines strongly modified the pHo sensitivity of G, while leaving Va unaffected (Fig. 4 A). However, exchanging the amino acids of the Cav2.1 DCS with those of Cav2.3 (Cav2.1(TEQE), Fig. 4 B) and vice et versa (Cav2.3(DEQN), not shown) affected neither G nor Va, suggesting that the DCS, as the EEEE locus, is involved in the pHo sensitivity of channel conductance, but is not responsible for the differential pHo sensitivity of the Cavα subunits. We then tested the pHo sensitivity of four chimeras in which each domain of the Cav2.1 subunit was sequentially exchanged with the corresponding domain of Cav2.3 (Cav2.1(EI, EII, EIII or EIV), Fig. 5). Only in the case of Cav2.1(EI), both G_x/G_7 and ΔVa values were significantly different from those of wild type Cav2.1 at all tested pHo (Tables 2

and 3). However, at alkaline pHo, the exchange of domain III (Cav2.1(EIII)) modified the pHo sensitivity of G, while leaving that of Va unaffected. The opposite effect was observed when domain IV was exchanged (Cav2.1(EIV), Fig. 5). Therefore, although the Cavα domain I is crucial for the pHo sensitivity, other regions of Cav2.3 could also be involved in modulating its pHo sensitivity.

The alignment of the sequences of the domain I of Cav2.1 and Cav2.3 (Fig. 6) shows that most of the differences are localized within the pore domain (segments S5 and S6 and the connecting P-loop), while the Voltage Sensor Domain (VSD, segments S1 to S4) appears to be more conserved. We therefore constructed two additional chimeras in which each of these regions of Cav2.1 was exchanged with the corresponding region of Cav2.3 (Cav2.1(pore-E) and Cav2.1(VSD-E), Figs. 7 A and 8 A). The G_x/G_7 values were not affected by the substitution of the VSD domain (Fig. 7 B), while they were significantly modified by the substitution of the pore domain (Fig. 8 B). Conversely, the ΔVa values were significantly modified by the substitution of the VSD domain (Fig. 7 C), but not by that of the pore domain (Fig. 8 C). These results indicate that the molecular determinants responsible for the pHo sensitivity of Va and G are localized within the VSD domain and within the pore domain, respectively. In several channels and receptors, protons have been shown to exert their effects by protonating histidines (see, for example [14]). The Cav2.3 domain I contains three histidines that are not present in Cav2.1 (two in the VSD domain and one in the pore domain, see Fig. 6). To investigate their potential role in the specific response to pHo variations, we sequentially mutated the histidines in the VSD (Cav2.3(H130/134A), Fig. 7 A) and in the pore domain of Cav2.3 (Cav2.3(H217A), Fig. 8A)) into alanines. Substitution of the VSD histidines did not affect G_x/G_7 (Fig. 7 B) but significantly modified the ΔVa values except at pHo = 10 (Fig. 7 C). On the other hand, substitution of the pore histidine did not affect ΔVa (Fig. 8 C), but modified significantly the G_x/G_7 values except at pHo between 6.5 and 8 (Fig. 8 B). Altogether, our results suggest that multiple amino acids of the domain I of Cav2.3 (including three non-conserved histidines) shape the pHo sensitivity of the activation potential and channel conductance.

DISCUSSION

A set of amino acids in the pore region mediates the pHo effect on channel conductance.

The glutamates of the Cavα EEEE locus are perfectly conserved in all HVA Ca^{2+} channels and ensure the selectivity of these channels for Ca^{2+} ions [29, 34]. In the Cav1.2 subunit these glutamates can be protonated at acidic pHo leading to partial block of ion fluxes and thus to inhibition of the macroscopic current [9, 20]. A proton-dependent decrease of channel selectivity has also been described in LVA T-type Ca^{2+} channels, which have, however, a different selectivity filter [11, 28]. Here, we demonstrate that pHo-induced variations of current amplitude can be in part attributed to changes in the channel conductance; however, the fact that extracellular protons affect differentially the conductance of Cav2.1 and 2.3 (Figs. 2 and 3) strongly suggests that amino acids outside the conserved EEEE locus mediate the pHo sensitivity of channel conductance. This hypothesis was also supported by works carried out on voltage-gated Na^+ channels in which the mutation of all the residues of the selectivity filter to alanine failed to completely abolish current inhibition by extracellular protons [27]. The more external DCS locus, which is specific to each Cavα subunit and is essential for the specific conductance of the different channels [8], is equivalent to the outer ring of carboxylates found in Na^+ channels. Mutations in this structure affect the sensitivity of Na^+ channels to pHo changes [19]. In the case of VGCC, the number of carboxylates at the DCS (Fig 4 A) rather than their spatial arrangement (from DEQN to TEQE, Fig 4 B), modified the pHo sensitivity of G. Like the EEEE locus, the DCS locus mediates, therefore, the effects of protons on the ion influx, but is not responsible for the specific pHo sensitivity of the different Cavα subunits. Our results indicate that residues of the S5-P-loop-S6 region of the Cavα domain I (Fig. 8), including a non-conserved histidine, are involved in precisely regulating the pHo sensitivity of each channel conductance. We thus propose that, like for Na^+ channels [21], the modulation of VGCC conductance by external protons is due to the combined titration of intra-pore and flanking amino acids. Our results support the idea that scattered residues in the outer vestibule may concentrate permeant ions at the pore mouth and that the resultant gradient is influenced, in a Cavα subunit-specific manner, by titration/protonation of key residues in the S5-P-loop-S6 segment of domain I leading to the modification of channel conductance.

A set of amino acids in the Voltage Sensor Domain mediates the pHo effect on channel gating.

The activation/opening of voltage-gated K^+, Na^+ or Ca^{2+} channels is linked to the movement of the S4 segment of each domain of the pore-forming subunit [1]. The precise

sequence of events and the molecular mechanisms leading from S4 movement to pore opening is still a matter of debate [31]. The depolarizing/hyperpolarizing shift of Va produced by extracellular acidosis/alkalosis [12] has been attributed to the screening of the extracellular surface charges and the consequent modification of the electric field across the plasma membrane in the vicinity of the channels [15]. Experiments on voltage-gated Na^+ channels inserted in artificial membranes [10] and our previous works on expressed Ca^{2+} channels [4] suggest that the surface charges that influence Va are carried by the channel protein itself (see also [36]). We found that domain I of the Cavα subunit is crucial for the specific pHo sensitivity of Va and identified two residues (H130 and H134) in the S3-S4 linker of Cav2.3 that are, at least in part, responsible for the pHo-induced Va shift (Fig. 7). These residues face the extracellular space and are therefore probably accessible to protons. They appear to be involved in the inhibition of Cav2.3 by Ni^+ ions [16] and application of Ni^+ to Cav2.1- or Cav2.3-expressing Xenopus oocytes produces a dose-dependent shift of Va that is reminiscent of the Va changes produced by pHo variations [35]. The equivalent histidine residue in Cav3.2 defines, with the neighbouring aspartate and glycine residues, a metal binding site implicated in the Ni^+ and Zn^{2+} inhibition of this channel [17, 18]. Metal chelation inhibits the gating charges and therefore the S4 movement and the subsequent pore opening [18]. A similar scenario could reasonably be imagined for the pHo modulation of Va in Cav2.3, but clearly, other residues within this and/or other channel domains (Figs. 5 and 7) are also involved in this effect.

In conclusion, here we show that the EEEE locus is not the only determinant that mediates the effects of extracellular protons on VGCC. We demonstrate that pHo-induced current amplitude changes do not result uniquely from the shift of activation potential, but also from a modification of channel conductance. We identified in the Cav2.3 domain I two sets of amino acids that are responsible of the sensitivity of Va and G to pHo variations.

ACKNOWLEDGMENTS

This work was supported by the “Centre Nationale de la Recherche Scientifique”, the “Institut Nationale de la Santé Et de la Recherche Médicale”, the “Fondation Simone & Cino Del Duca”, the “Fondation pour la Recherche sur le Cerveau”.

We thank T. Snutch and E. Perez-Reyes for kindly providing calcium channels cDNAs, J-M. Donnay and J-C Mazur for oocyte preparations.

REFERENCES

1. Bezanilla F (2008) How membrane proteins sense voltage. Nat Rev Mol Cell Biol 9:323-332
2. Carlin KP (2005) Modulation of calcium currents in mouse ventral horn neurons by extracellular pH. Eur J Neurosci 22:2655-2660
3. Catterall WA (1998) Structure and function of neuronal Ca2+ channels and their role in neurotransmitter release. Cell Calcium 24:307-323
4. Cens T, Dalle C, Charnet P (1998) Expression of beta subunit modulates surface potential sensing by calcium channels. Pflugers Arch 435:865-867
5. Cens T, Leyris JP, Charnet P (2008) Introduction into Ca(v)2.1 of the homologous mutation of Ca(v)1.2 causing the Timothy syndrome questions the role of V421 in the phenotypic definition of P-type Ca(2+) channel. Pflugers Arch 457:417-430
6. Cens T, Mangoni ME, Nargeot J, Charnet P (1996) Modulation of the alpha 1A Ca2+ channel by beta subunits at physiological Ca2+ concentration. FEBS Lett 391:232-237
7. Cens T, Restituito S, Rousset M, Charnet P (2005) Role of β subunits in voltage-gated calcium channel functions. In: Zamponi GW (ed) Voltage Gated Calcium Channels. Landes Bioscience, Georgetown, Texas, USA, p 95-112
8. Cens T, Rousset M, Kajava A, Charnet P (2007) Molecular determinant for specific ca/ba selectivity profiles of low and high threshold Ca2+ channels. J Gen Physiol 130:415-425
9. Chen XH, Bezprozvanny I, Tsien RW (1996) Molecular basis of proton block of L-type Ca2+ channels. J Gen Physiol 108:363-374
10. Cukierman S, Zinkand WC, French RJ, Krueger BK (1988) Effects of membrane surface charge and calcium on the gating of rat brain sodium channels in planar bilayers. J Gen Physiol 92:431-447
11. Delisle BP, Satin J (2000) pH modification of human T-type calcium channel gating. Biophys J 78:1895-1905
12. Doering CJ, McRory JE (2007) Effects of extracellular pH on neuronal calcium channel activation. Neuroscience 146:1032-1043
13. Du J, Xie J, Yue L (2009) Modulation of TRPM2 by acidic pH and the underlying mechanisms for pH sensitivity. J Gen Physiol 134:471-488
14. Goodchild SJ, Lamy C, Seutin V, Marrion NV (2009) Inhibition of K(Ca)2.2 and K(Ca)2.3 channel currents by protonation of outer pore histidine residues. J Gen Physiol 134:295-308

15. Green WN, Anderson OS (1991) Surface charges and ion channel function. Annu Rev Physiol 53:341-359
16. Kang HW, Moon HJ, Joo SH, Lee JH (2007) Histidine residues in the IS3-IS4 loop are critical for nickel-sensitive inhibition of the Cav2.3 calcium channel. FEBS Lett 581:5774-5780
17. Kang HW, Park JY, Jeong SW, Kim JA, Moon HJ, Perez-Reyes E, Lee JH (2006) A molecular determinant of nickel inhibition in Cav3.2 T-type calcium channels. J Biol Chem 281:4823-4830
18. Kang HW, Vitko I, Lee SS, Perez-Reyes E, Lee JH (2010) Structural Determinants of the High Affinity Extracellular Zinc Binding Site on Cav3.2 T-type Calcium Channels. J Biol Chem 285:3271-3281
19. Khan A, Romantseva L, Lam A, Lipkind G, Fozzard HA (2002) Role of outer ring carboxylates of the rat skeletal muscle sodium channel pore in proton block. J Physiol 543:71-84
20. Klockner U, Mikala G, Schwartz A, Varadi G (1996) Molecular studies of the asymmetric pore structure of the human cardiac voltage-dependent Ca2+ channel. J Biol Chem 271:22293-22296
21. Li RA, Velez P, Chiamvimonvat N, Tomaselli GF, Marban E (2000) Charged Residues between the Selectivity Filter and S6 Segments Contribute to the Permeation Phenotype of the Sodium Channel. J Gen Physiol 115:81-92
22. Pinchenko VO, Kostyuk PG, Kostyuk EP (2005) Influence of external pH on two types of low-voltage-activated calcium currents in primary sensory neurons of rats. Biochim Biophys Acta 1724:1-7
23. Richards KS, Swensen AM, Lipscombe D, Bommert K (2007) Novel CaV2.1 clone replicates many properties of Purkinje cell CaV2.1 current. Eur J Neurosci 26:2950-2961
24. Sather WA, McCleskey EW (2003) Permeation and selectivity in calcium channels. Annu Rev Physiol 65:133-159
25. Shah MJ, Meis S, Munsch T, Pape HC (2001) Modulation by extracellular pH of low- and high-voltage-activated calcium currents of rat thalamic relay neurons. J Neurophysiol 85:1051-1058
26. Smirnov SV, Knock GA, Belevych AE, Aaronson PI (2000) Mechanism of effect of extracellular pH on L-type Ca(2+) channel currents in human mesenteric arterial cells. Am J Physiol Heart Circ Physiol 279:H76-H85

27. Sun YM, Favre I, Schild L, Moczydlowski E (1997) On the Structural Basis for Size-selective Permeation of Organic Cations through the Voltage-gated Sodium Channel: Effect of Alanine Mutations at the DEKA Locus on Selectivity, Inhibition by Ca2+ and H+, and Molecular Sieving. J Gen Physiol 110:693-715
28. Talavera K, Janssens A, Klugbauer N, Droogmans G, Nilius B (2003) Extracellular Ca2+ modulates the effects of protons on gating and conduction properties of the T-type Ca2+ channel alpha1G (CaV3.1). J Gen Physiol 121:511-528
29. Tang S, Mikala G, Bahinski A, Yatani A, Varadi G, Schwartz A (1993) Molecular localization of ion selectivity sites within the pore of a human L-type cardiac calcium channel. J Biol Chem 268:13026-13029
30. Tombaugh GC, Somjen GG (1996) Effects of extracellular pH on voltage-gated Na+, K+ and Ca2+ currents in isolated rat CA1 neurons. J Physiol 493:719-732
31. Tombola F, Pathak MM, Isacoff EY (2006) How does voltage open an ion channel? Annu Rev Cell Dev Biol 22:23-52
32. Vacher H, Mohapatra DP, Trimmer JS (2008) Localization and targeting of voltage-dependent ion channels in mammalian central neurons. Physiol Rev 88:1407-1447
33. Xiong ZQ, Stringer JL (2000) Extracellular pH responses in CA1 and the dentate gyrus during electrical stimulation, seizure discharges, and spreading depression. J Neurophysiol 83:3519-3524
34. Yang J, Ellinor PT, Sather WA, Zhang JF, Tsien RW (1993) Molecular determinants of Ca2+ selectivity and ion permeation in L-type Ca2+ channels. Nature 366:158-161
35. Zamponi GW, Bourinet E, Snutch TP (1996) Nickel block of a family of neuronal calcium channels: subtype- and subunit-dependent action at multiple sites. J Membr Biol 151:77-90
36. Zamponi GW, Snutch TP (1996) Evidence for a specific site for modulation of calcium channel activation by external calcium ions. Pflugers Arch 431:470-472
37. Zhou W, Jones SW (1995) Surface charges and calcium channel saturation in bullfrog sympathetic neurons. J Gen Physiol 105:441-462

FIGURE LEGENDS.

Figure 1. Traces of current and current-voltage curves obtained for wild type Cav2.1 (A) and Cav2.3 (B) at different extracellular pH (pHo). Currents were elicited by applying 400 ms-long depolarization steps from -60 to +40 mV from a holding potential of -100mV using Ba^{2+} solution at pHo = 6, 7 or 8. Dotted lines represent the zero current level. Scale bar = 500nA for Cav2.1 and 200nA for Cav2.3. The current-voltage curves at pHo = 6 (squares), 7 (circles) and 8 (triangles) were normalized to the maximum peak current amplitude measured at pHo = 7. The ratios of the peak current amplitudes measured at pHo = 6 or 8 and at pHo = 7 for Cav2.1 (0.72±0.01, n = 4, and 1.02±0.09, n = 4, respectively) were significantly different from those obtained for Cav2.3 (0.38±0.01, n = 9, and 1.21±0.05, n = 7, respectively, $p<0.05$).

Figure 2. Single channel current properties of Cav2.3 at different pHo. (A) Representative traces of unitary currents elicited by depolarization steps from -100 mV to -20 mV using Ba^{2+} extracellular solutions at pHo = 7 or 10 (left) and the corresponding current-voltage curves with superimposed linear regressions (right). The shift of the activation potential led to a higher open probability at pHo = 10 than at pHo = 7. Scale bars: 40 ms and 2 pA. (B) Single channel open time distributions measured at -20 mV and 0 mV were marginally affected by the pHo change from 7 to 10. Mean τfast = 0.56±0.10 and 0.47±0.08 ms at -20 mV and 0.36±0.05 and 0.59±0.06 ms at 0mV, at pHo = 7 and 10, respectively. Mean τslow = 2.88±0.71 and 2.43±0.41 ms at -20 mV and 2.21±0.41 and 2.37±0.66 at 0 mV, at pHo = 7 and 10, respectively. (C) The mean of the unitary conductance values obtained from 8-16 oocytes shows a 50% increase between pHo = 7 and 10.* denotes a significant difference ($p < 0.05$).

Figure 3. Cav2.1 and Cav2.3 currents obtained with voltage ramps at different pHo. (A) Wild type Cav2.1 and Cav2.3 Ba^{2+} currents were elicited by applying 400 ms-long voltage ramps from -80 to +80 mV from a holding potential of -100mV using solutions at pHo = 6, 6.5, 7 (bold trace), 7.5, 8, 8.5, 9 and 10. Dotted lines represent the zero current level. The outward currents were deleted for clarity. Scale bars = 200 nA. (B) Conductance ratio (G_x/G_7) obtained by dividing the maximal whole-cell conductance obtained at different pHo by the value at pHo = 7 for Cav2.3 (circles) and Cav2.1 (squares) reported against the pHo values. (C) Shift of the activation potential (ΔVa) determined by the difference between the Va at the indicated

pHo and at pHo = 7 for Cav2.1 and Ca2.3. * denotes a significant difference between wild type Cav2.1 and wild type Cav2.3 ($p < 0.05$).

Figure 4. Role of the Divalent Cation Selectivity (DCS) locus in the pHo sensitivity. Traces of current (top), G_x/G_7 (middle) and ΔVa (bottom) values were obtained as in Fig. 3. (A) The mutation of all the amino acids of the Cav2.3 DCS to alanines (Cav2.3(AAAA)) strongly modified the pHo-sensitivity of G, but not that of Va. (B) The substitution of the amino acids of the Cav2.1 DCS with those of Cav2.3 (Cav2.1(TEQE)), had no effects on the pHo sensitivity of both Va and G. The dashed line and the dotted line on the graphs represent the curves obtained for wild type Cav2.1 and wild type Cav2.3 in Fig. 3, respectively. # denotes a significant difference between Cav2.3(AAAA) and wild type Cav2.3 ($p < 0.05$). Scale bars = 200 nA.

Figure 5. Role of the Cav2.3 domain I in pHo sensitivity. G_x/G_7 (left panels) and ΔVa (right panels) values were obtained as in Fig. 3. Each domain of Cav2.1 was exchanged with the corresponding Cav2.3 domain (Cav2.1(EI to EIV) from top to bottom). The exchange of the domain I modified the pHo sensitivity of both Va and G. The dashed line and the dotted line on the graphs represent the curves obtained for wild type Cav2.1 and wild type Cav2.3 in Fig. 3, respectively. * denotes a significant difference vs wild type Cav2.1 ($p < 0.05$).

Figure 6. Alignment of the amino acid sequences of the domain I of Cav2.1 and Cav2.3. Boxes delineate the transmembrane segments (S1 to S6). Most of the differences in the two sequences are localized in the P-loop (between segment S5 and S6). The residues of the EEEE and DCS loci are underlined. In bold, the two histidines in the S3-S4 linker and the histidine in the P-loop that are Cav2.3-specific and were mutated in this study. The arrow indicates where the EcoRI restriction site has been introduced to produce the chimeras Cav2.1(pore-E) and Cav2.1(VSD-E).

Figure 7. Role of the VSD of domain I in the pHo sensitivity of Va. (A) The substitution of the VSD of Cav2.1 with the corresponding domain of Cav2.3 (Cav2.1(VSD-E)) and the mutation of the two non-conserved histidines of the VSD of the Cav2.3 domain I into alanines (Cav2.3(H130/134A)) demonstrated the role of the VSD residues in the pHo sensitivity of Va. (B) G_x/G_7 values were obtained as in Fig. 3. None of the modifications in Cav2.1 and Cav2.3 affected the pHo-sensitivity of G. The dashed line and the dotted line on the graph represent

the curves obtained for wild type Cav2.1 and wild type Cav2.3 in Fig. 3, respectively. (C) ΔVa values obtained as in Fig.3. The magnitude of the Va shift was significantly modified in Cav2.1(VSD-E) compared to wild type Cav2.1 at all pHo tested (*, $p < 0.05$), while for Cav2.3(H130/134A) the shift was significantly modified at all pHo, except pHo = 10, compared to wild type Cav2.3 (#, $p < 0.05$).

Figure 8. Role of the pore region of domain I in the pHo sensitivity of G. (A) The substitution of the pore region of Cav2.1 with the corresponding region of Cav2.3 (Cav2.1(pore-E)) and the mutation of the single non-conserved histidine of the Cav2.3 pore region into alanine (Cav2.3(H217A)) demonstrated the role of the pore residues in the pHo sensitivity of G. (B) G_x/G_7 values obtained as in Fig. 3. The two modifications changed significantly the pHo sensitivity of G. The dashed line and the dotted line on the graph represent the curves obtained for wild type Cav2.1 and wild type Cav2.3 in Fig. 3, respectively. (C) ΔVa values were determined as in Fig. 3. Except for Cav2.1(pore-E) at pHo =6, both modifications did not affect ΔVa. * and # denotes a significant difference between wild type Cav2.1 and Cav2.1(pore-E) or wild type Cav2.3 and Cav2.3(H217A), respectively ($p < 0.05$).

Table 1. Parameters (in mV) of the current-voltage curves determined for wild type Cav2.1 and Cav2.3 at different extracellular pHo.

Traces of current were obtained with square pulses or voltage ramps and fitted with a Boltzmann's equation as described in the Materials and Methods section. *Va* is the potential for half activation, *k* is a slope factor and *Erev* is the reversal potential. All values are means ± SEM of *n* determinations. Note that the values obtained with square pulses or voltage ramps for both Cavα subunits are similar at each pHo.

	pHo = 6		pHo = 7		pHo = 8	
Cav2.3	pulse (n = 9)	ramp (n = 13)	pulse (n = 7)	ramp (n = 8)	pulse (n = 12)	ramp (n = 8)
Va	13.1±0.9[a]	14.7±0.7[a]	-3.8±1.2	-1.4±1.1	-9.6±1.2[a]	-7.8±1.1[a]
k	-5.3±0.1[a]	-5.7±0.1[a]	-5.1±0.2	-4.9±0.2	-5.0±0.1	-4.6±0.2
Erev	57±1	57±1	55±1	55±1	53±1	53±1
	pHo = 6		pHo = 7		pHo = 8	
Cav2.1	pulse (n = 9)	ramp (n = 13)	pulse (n = 8)	ramp (n = 13)	pulse (n = 7)	ramp (n = 13)
Va	-2.1±1.4[a]	0.1±0.7[a]	-6.1±1.0	-5.8±0.8	-10.7±2.0[a]	-8.2±0.8[a]
k	-4.4±0.1	-4.3±0.1	-4.2±0.3	-4.1±0.1	-4.1±0.3	-4.1±0.1
Erev	49±1	47±1	49±1	47±1	50±1	47±1

[a] significantly different from the values determined at pHo = 7 ($p<0.05$).

Table 2 Comparison of the magnitude of activation potential shift (ΔVa in mV) obtained for wild type and mutated Cavα subunits at different pHo.

Traces of current were obtained with voltage ramps and fitted with a Boltzmann's equation as described in the Materials and Methods section. ΔVa is the difference between the activation potential at the indicated pHo and at pHo = 7. The values obtained for wild type Cav2.1 and Cav2.3 when using square pulses rather than voltages ramps are given in parentheses. Note that these values are similar for both channels. All values are means ± SEM of *n* determinations.

ΔVa(mV)	*n*	pHo = 6	pHo = 6.5	pHo = 7.5	pHo = 8	pHo = 8.5	pHo = 9	pHo = 10
Cav2.1	16 (9)	+5.5±0.6 (+6.2±0.5)	+2.3±0.1	-1.2±0.1	-2.0±0.2 (-1.8±0.3)	-2.4±0.2	-4.3±0.3	-8.7±0.5
Cav2.1(TEQE)	9	+7.0±0.2	+2.1±0.1	-1.1±0.1	-1.9±0.1	-2.6±0.1	-4.0±0.1	-8.7±0.4
Cav2.1(EI)	9	+8.0±0.8[a]	+4.0±0.2[a]	-2.3±0.2[a]	-2.9±0.5[a]	-4.5±0.4[a]	-6.3±0.3[a]	-13.7±0.6[a]
Cav2.1(EII)	12	+6.4±0.4	+3.1±0.1[a]	-0.8±0.1[a]	-1.9±0.3	-2.4±0.2	-3.6±0.3	-8.0±0.9
Cav2.1(EIII)	4	+4.4±0.2	+1.9±0.1	-1.4±0.5	-1.9±0.2	-2.9±0.2	-4.6±0.2	-9.9±0.7
Cav2.1(EIV)	7	+6.2±0.4	+2.9±0.2	-1.7±0.4	-2.4±0.2	-3.6±0.2[a]	-6.2±0.4[a]	-12.7±0.5[a]
Cav2.1(pore-E)	19	+6.9±0.2[a]	+2.3±0.1	-1.2±0.1	-2.1±0.2	-2.8±0.1	-4.5±0.2	-9.6±0.3
Cav2.1(VSD-E)	18	+11.9±0.3[a]	+4.6±0.1[a]	-2.2±0.1[a]	-3.8±0.1[a]	-5.0±0.2[a]	-6.4±0.2[a]	-12.0±0.4[a]
Cav2.3	10 (11)	+15.0±0.7 (+15.3±0.9)	+6.6±0.2	-4.0±0.1	-6.4±0.2 (-5.8±0.2)	-8.4±0.3	-11.8±0.3	-18.6±0.5
Cav2.3(AAAA)	7	+13.2±0.8	+6.3±0.2	-3.9±0.3	-6.8±0.2	-9.1±0.3	-12.0±0.4	-18.1±0.6
Cav2.3(H130/134A)	15	+11.1±0.3[b]	+4.9±0.1[b]	-3.3±0.1[b]	-5.3±0.2[b]	-6.8±0.3[b]	-10.6±0.3[b]	-18.8±0.6
Cav2.3(H217A)	7	+15.1±0.5	+5.9±0.3	-3.6±0.1	-6.2±0.2	-8.2±0.2	-11.0±0.2	-17.4±0.5

[a] significantly different from wild type Cav2.1 ($p<0.05$).

[b] significantly different from wild type Cav2.3 ($p<0.05$).

Table 3. Comparison of the conductance ratio (G_x/G_7) obtained for wild type and mutated Cavα subunits at different pHo.

Traces of current obtained with voltage ramps were fitted with a modified Boltzmann's equation as described in the Materials and Methods section. G_x/G_7 is the ratio between the maximal whole-cell conductance G at the indicated pHo and at pHo = 7. The values obtained for wild type Cav2.1 and Cav2.3 when using square pulses rather than voltage ramps are given in parentheses. Note that these values are similar for both channels. All values are means ± SEM of *n* determinations.

G_x/G_7	*n*	pHo = 6	pHo = 6.5	pHo = 7.5	pHo = 8	pHo = 8.5	pHo = 9	pHo = 10
Cav2.1	16 (4)	0.85±0.02 (076±0.04)	0.94±0.01	1.02±0.01	1.02±0.01 (0.98±0.05)	1.01±0.02	1.00±0.02	1.01±0.02
Cav2.1(TEQE)	9	0.80±0.01	0.92±0.01	1.03±0.01	1.04±0.01	1.04±0.02	1.03±0.03	1.00±0.05
Cav2.1(EI)	9	0.77±0.02[a]	0.89±0.01[a]	1.07±0.01[a]	1.11±0.03[a]	1.13±0.03[a]	1.15±0.02[a]	1.13±0.04[a]
Cav2.1(EII)	10	0.87±0.01	0.94±0.01	1.01±0.01	1.01±0.01	1.01±0.01	1.02±0.01	1.03±0.01
Cav2.1(EIII)	4	0.86±0.02	0.94±0.01	1.00±0.01	1.00±0.01	0.98±0.01	0.94±0.01[a]	0.85±0.01[a]
Cav2.1(EIV)	7	0.83±0.02	0.93±0.01	1.01±0.01	1.01±0.01	1.01±0.01	1.00±0.01	0.98±0.01
Cav2.1(pore-E)	19	0.76±0.02[a]	0.89±0.01[a]	1.06±0.01[a]	1.13±0.02[a]	1.16±0.02[a]	1.17±0.03[a]	1.18±0.06[a]
Cav2.1(VSD-E)	15	0.83±0.01	0.94±0.01	1.01±0.01	1.02±0.01	1.03±0.01	1.03±0.02	1.00±0.02
Cav2.3	10 (9)	0.61±0.01 (0.56±0.03)	0.83±0.01	1.08±0.01	1.11±0.01 (1.10±0.03)	1.12±0.02	1.12±0.02	1.10±0.01
Cav2.3(AAAA)	7	0.72±0.04[b]	0.88±0.02	1.08±0.01	1.16±0.03	1.23±0.05[b]	1.29±0.06[b]	1.34±0.08[b]
Cav2.3(H130/134A)	15	0.66±0.01	0.85±0.01	1.06±0.01	1.11±0.02	1.12±0.02	1.12±0.03	1.11±0.04
Cav2.3(H217A)	7	0.68±0.01[b]	0.86±0.01	1.06±0.01	1.16±0.01	1.22±0.02[b]	1.28±0.03[b]	1.29±0.05[b]

[a] significantly different from wild type Cav2.1 ($p<0.05$).

[b] significantly different from wild type Cav2.3 ($p<0.05$).

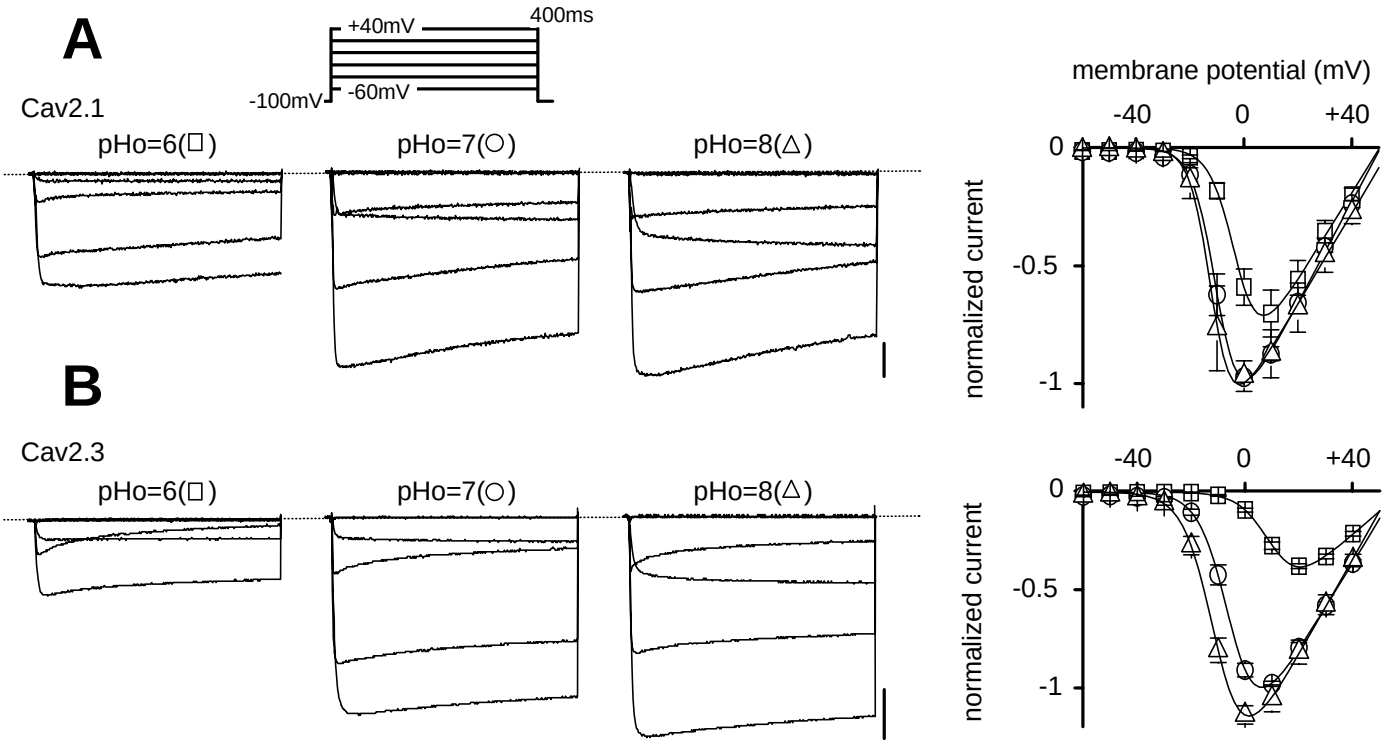
A
+40mV
400ms
-100mV
-60mV
Cav2.1
pHo=6(□)
pHo=7(○)
pHo=8(△)
B
Cav2.3
pHo=6(□)
pHo=7(○)
pHo=8(△)
membrane potential (mV)
-40
0
+40
0
-0.5
-1
normalized current
-40
0
+40
0
-0.5
-1
normalized current

Figure 1

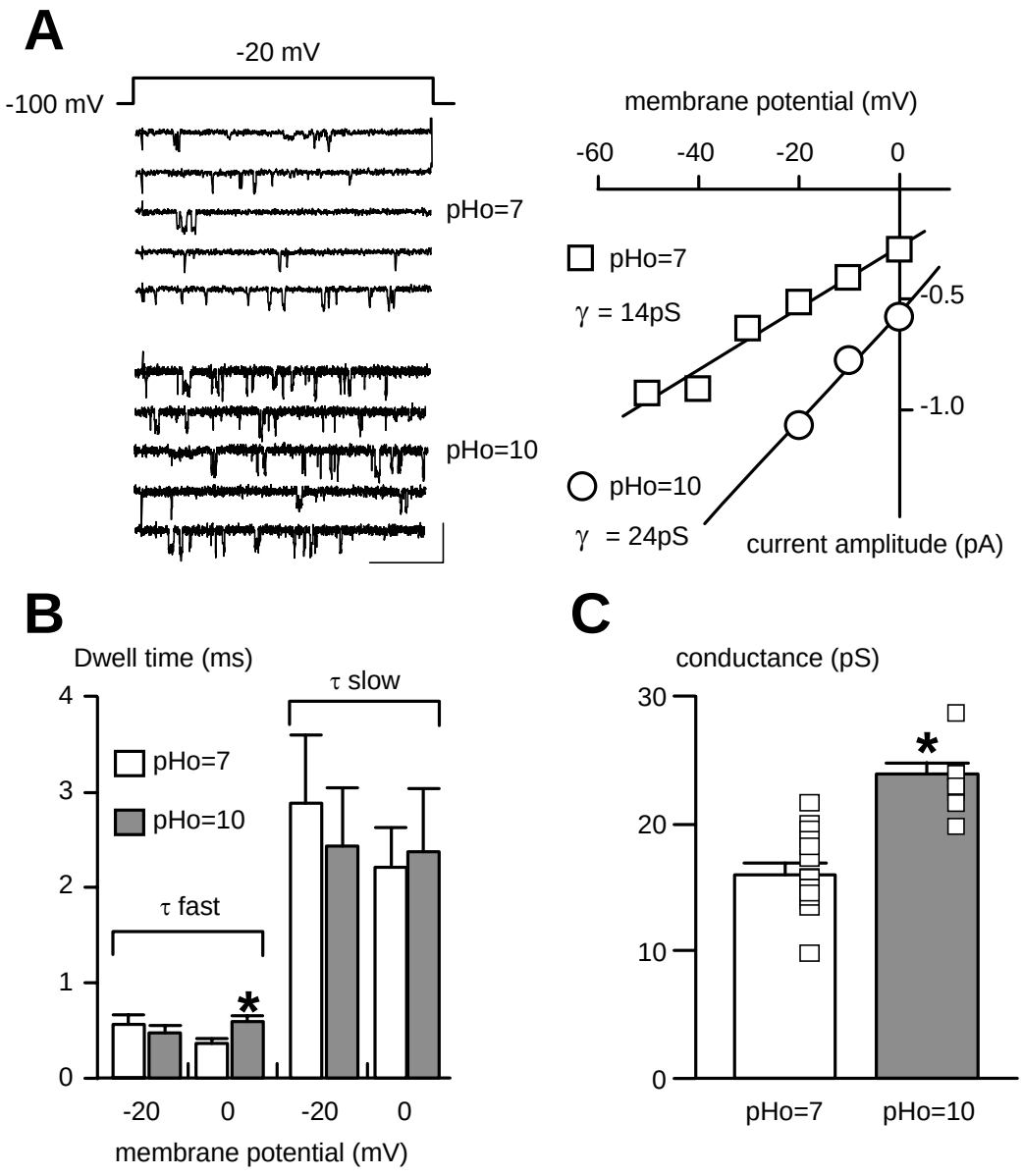
A
-20 mV
-100 mV
pHo=7
pHo=10
membrane potential (mV)
-60
-40
-20
0
pHo=7
γ = 14pS
-0.5
-1.0
pHo=10
γ = 24pS
current amplitude (pA)
B
Dwell time (ms)
τ slow
τ fast
pHo=7
pHo=10
4
3
2
1
0
-20
0
-20
0
membrane potential (mV)
C
conductance (pS)
30
20
10
0
pHo=7
pHo=10

Figure 2

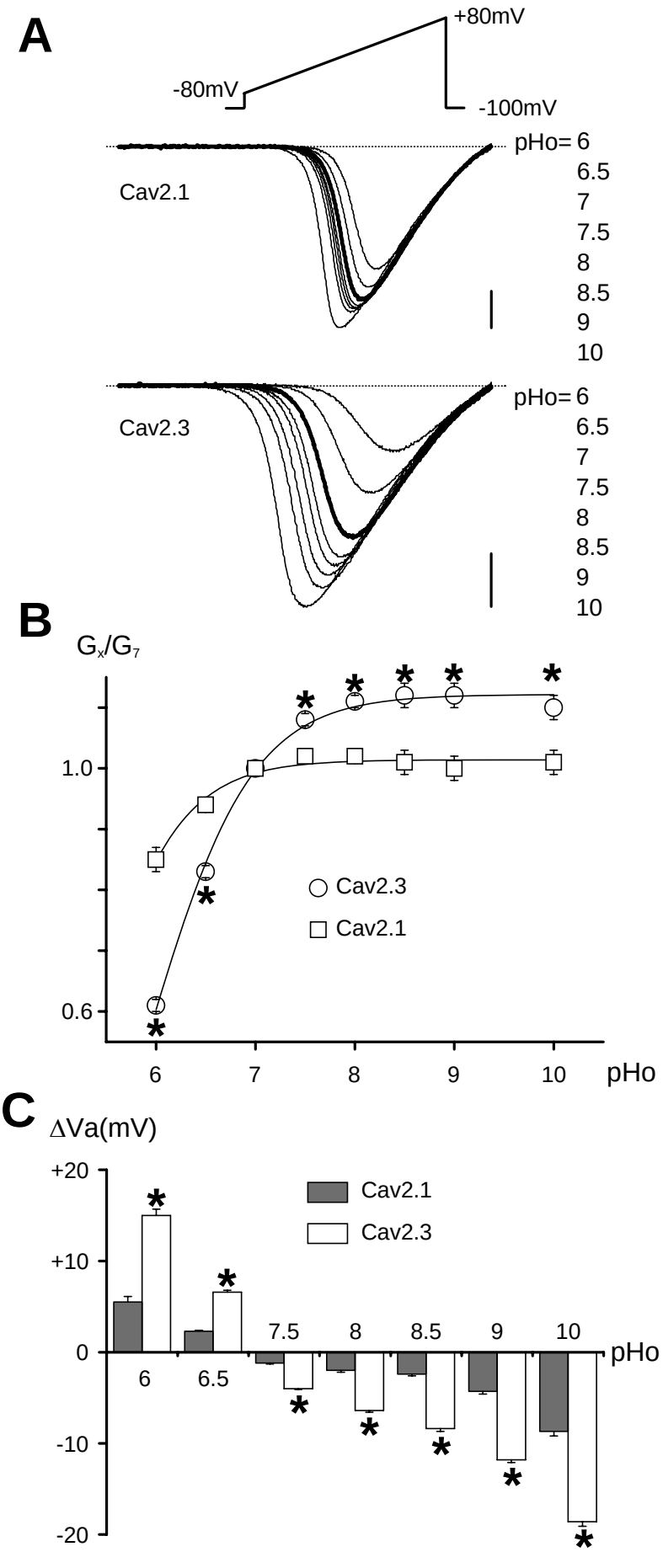
A
+80mV
-80mV
-100mV
pHo= 6
6.5
7
7.5
8
8.5
9
10
Cav2.1
Cav2.3
B
G_x/G_7
1.0
0.6
Cav2.3
Cav2.1
6
7
8
9
10
pHo
C
ΔVa(mV)
+20
+10
0
-10
-20
Cav2.1
Cav2.3
6
6.5
7.5
8
8.5
9
10
pHo

Figure 3

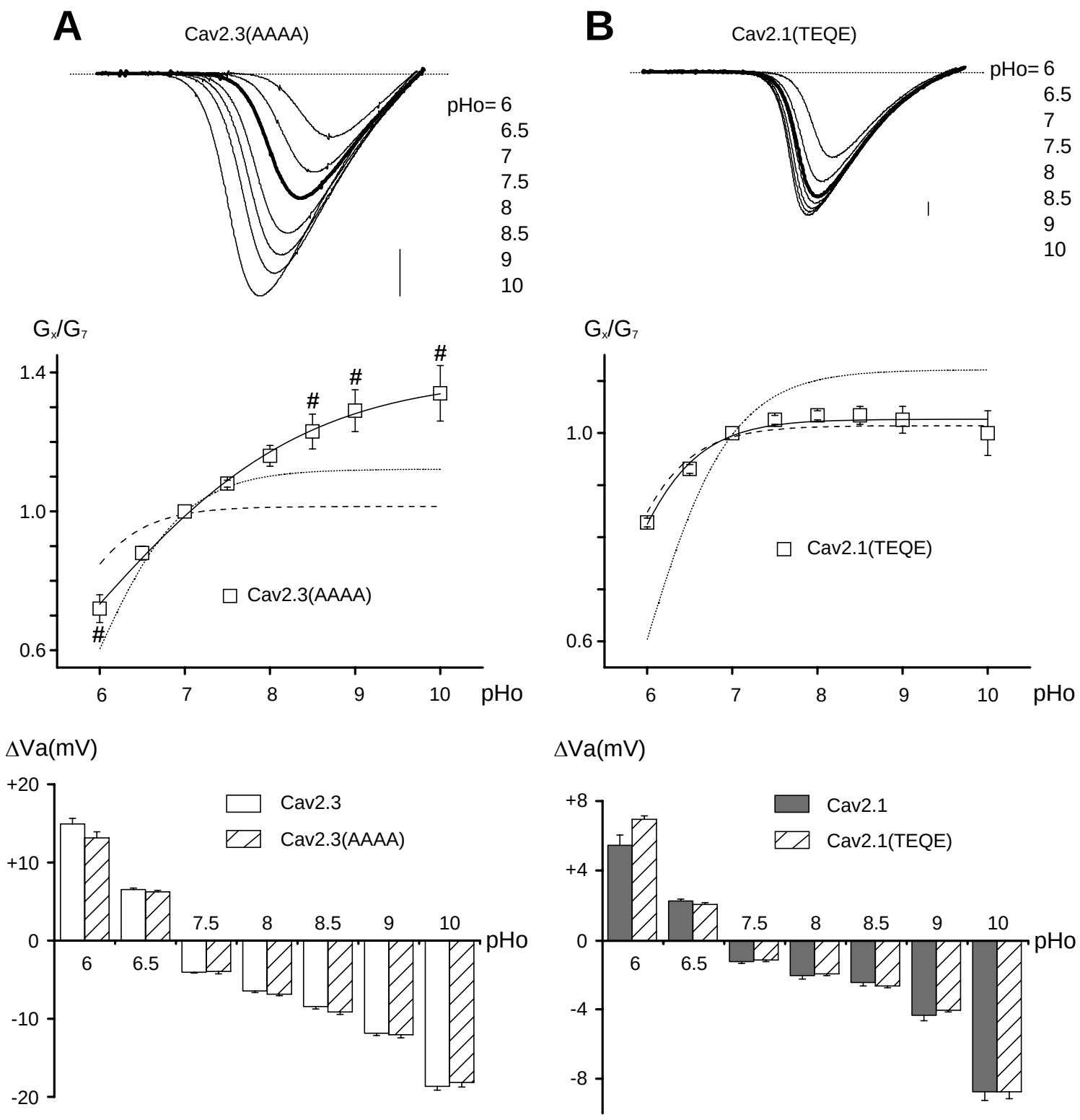
A
Cav2.3(AAAA)
pHo= 6
6.5
7
7.5
8
8.5
9
10
B
Cav2.1(TEQE)
pHo= 6
6.5
7
7.5
8
8.5
9
10
Gx/G7
1.4
1.0
0.6
#
#
#
#
Cav2.3(AAAA)
6
7
8
9
10
pHo
Gx/G7
1.0
0.6
Cav2.1(TEQE)
6
7
8
9
10
pHo
ΔVa(mV)
+20
+10
0
-10
-20
Cav2.3
Cav2.3(AAAA)
6
6.5
7.5
8
8.5
9
10
pHo
ΔVa(mV)
+8
+4
0
-4
-8
Cav2.1
Cav2.1(TEQE)
6
6.5
7.5
8
8.5
9
10
pHo

Figure 4

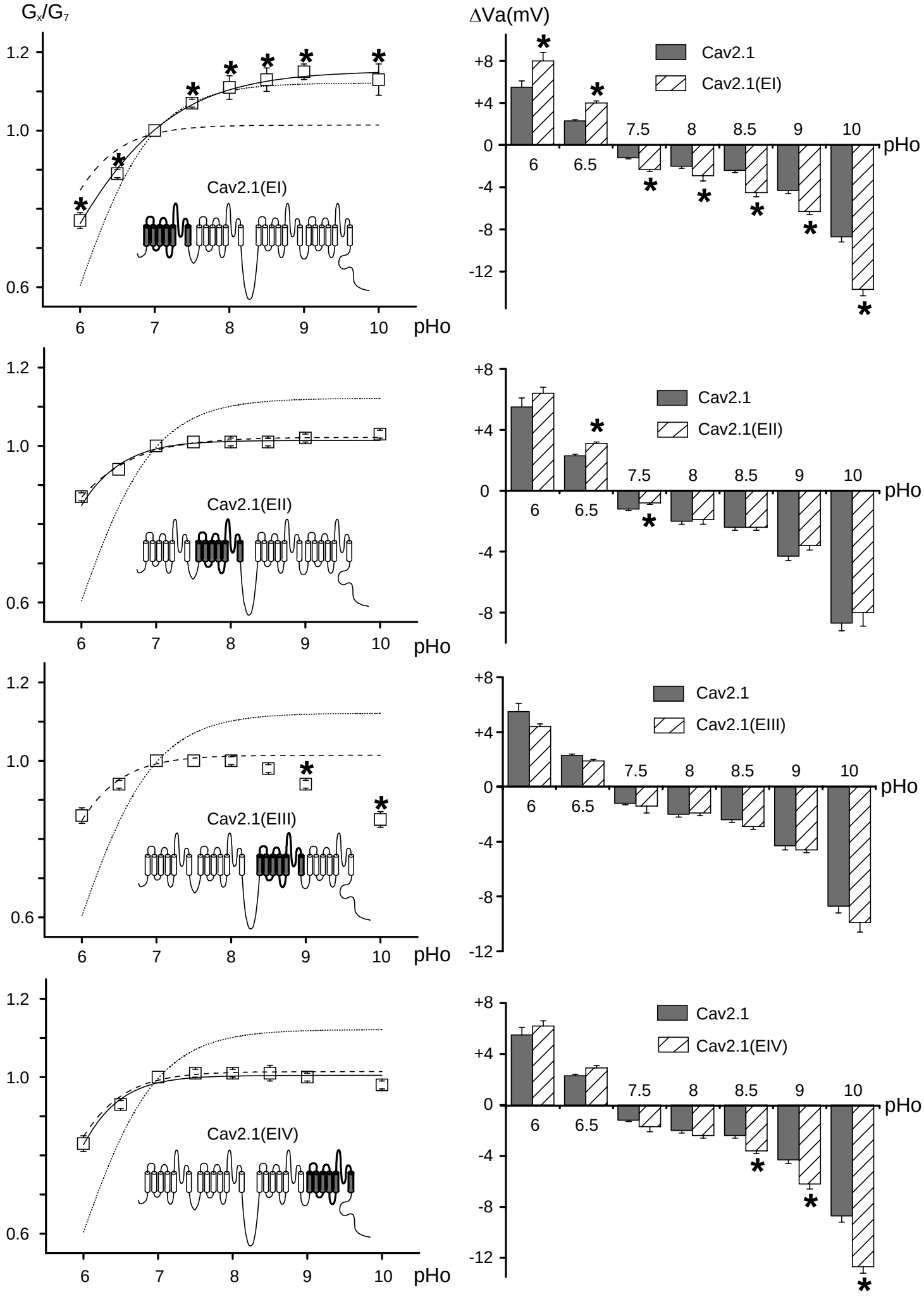
G_x/G_7
1.2
1.0
0.6
Cav2.1(EI)
6
7
8
9
10
pHo
ΔVa(mV)
+8
+4
0
-4
-8
-12
Cav2.1
Cav2.1(EI)
6
6.5
7.5
8
8.5
9
10
pHo
Cav2.1(EII)
Cav2.1(EIII)
Cav2.1(EIV)

Figure 5


Cav2.1 (100) PPFEYMILATIIANCIVLALEQHLPDDDKTPMSERLDDTEPYFIGIFCFE
Cav2.3 (40) ----------E-------R--EK----------
S1
S2
Cav2.1 AGIKIVALGFAFHKGSYLRNGWNVMDFVVVLTGILATVGTEF DLRT
Cav2.3 ----------I---------I---S-----A--H-NTHV----
S3
Cav2.1 LRAVRVLRPLKLVSGIPSLQVVLKSIMKAMIPLLQIGLLLFFAILIFAII
Cav2.3 ----------I---------V----------M----
S4
S5
Cav2.1 GLEFYMGKFHTTCFEEGTDDIQGESP APCGTEEPARTCPNGTKCQPYWE
Cav2.3 -----S--L-RA--MNNSGILE-FD-PH---VQG --A-YE-K D-I
Cav2.1 GPNNGITQFDNILFAVLTVFQCITMEGWTDLLYNSNDASGNTWNWLYFIP
Cav2.3 ---D----------TV---T---L-A--------
Cav2.1 LIIIGSFFMLNLVLGVL (360)
Cav2.3 --------V-------- (300)
S6

Figure 6

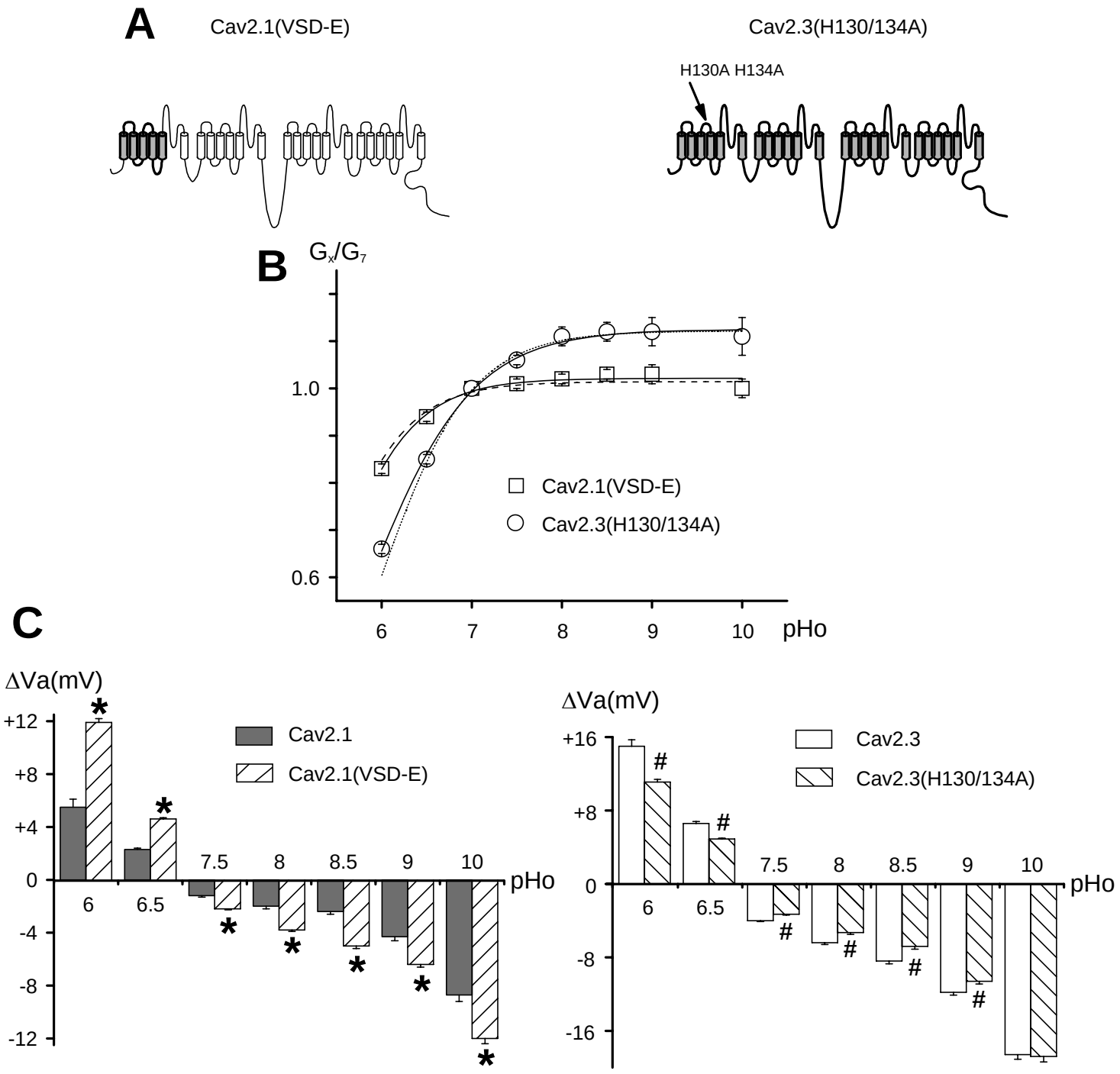
A
Cav2.1(VSD-E)
Cav2.3(H130/134A)
H130A H134A
B
G_x/G_7
1.0
0.6
6
7
8
9
10
pHo
Cav2.1(VSD-E)
Cav2.3(H130/134A)
C
ΔVa(mV)
+12
+8
+4
0
-4
-8
-12
Cav2.1
Cav2.1(VSD-E)
6
6.5
7.5
8
8.5
9
10
pHo
ΔVa(mV)
+16
+8
0
-8
-16
Cav2.3
Cav2.3(H130/134A)
#
*

Figure 7

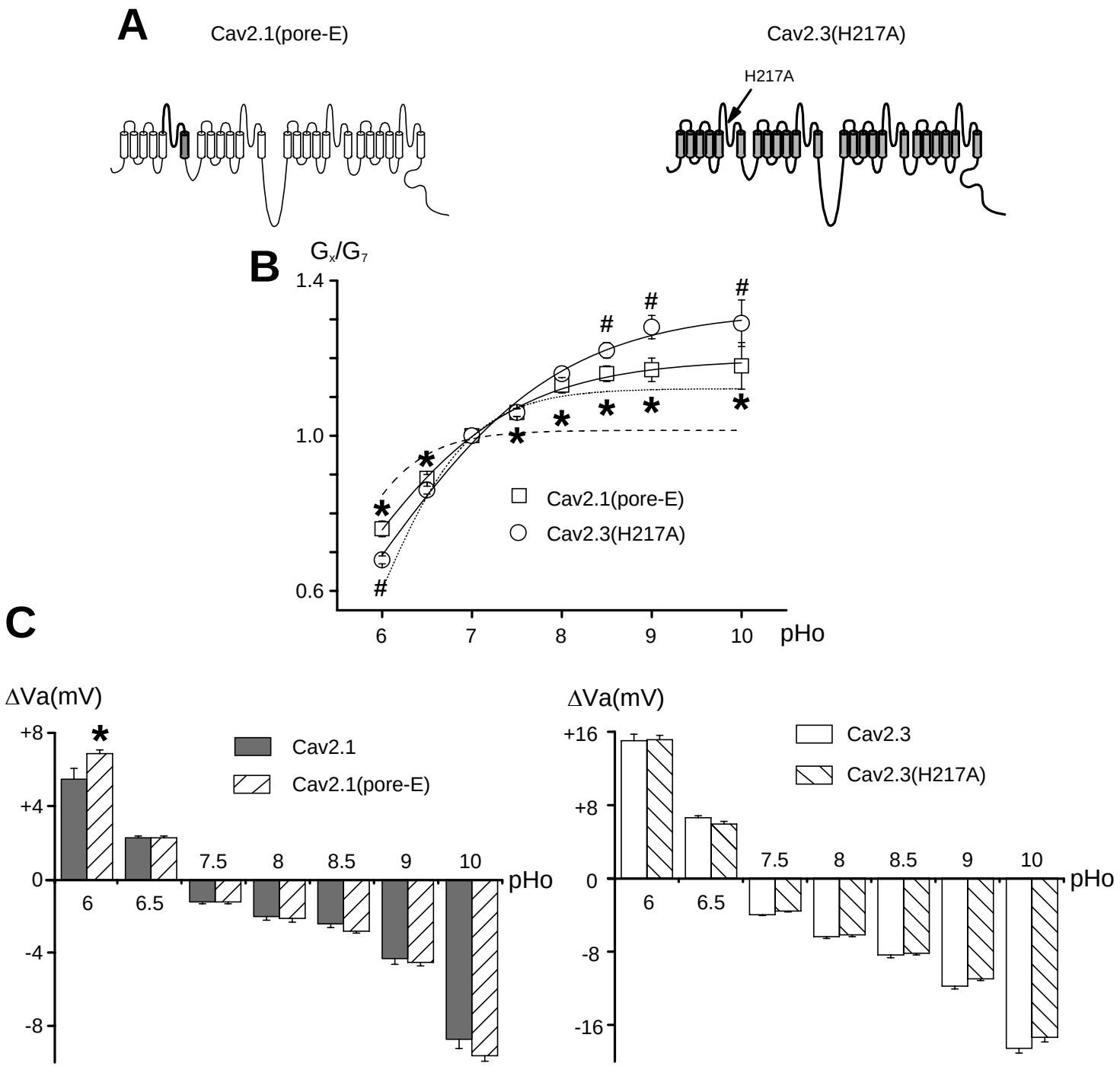
A
Cav2.1(pore-E)
Cav2.3(H217A)
H217A
B
G_x/G_7
1.4
1.0
0.6
6
7
8
9
10
pHo
Cav2.1(pore-E)
Cav2.3(H217A)
C
ΔVa(mV)
+8
+4
0
-4
-8
Cav2.1
Cav2.1(pore-E)
6
6.5
7.5
8
8.5
9
10
pHo
ΔVa(mV)
+16
+8
0
-8
-16
Cav2.3
Cav2.3(H217A)
6
6.5
7.5
8
8.5
9
10
pHo

Figure 8